

Vorticity and Particle Polarization in Relativistic Heavy-Ion Collisions

Yu. B. Ivanov,^{1,2,3,*} V. D. Toneev,¹ and A. A. Soldatov²

¹*Bogoliubov Laboratory for Theoretical Physics, Joint Institute for Nuclear Research, Dubna 141980, Russia*

²*National Research Nuclear University "MEPhI", Moscow 115409, Russia*

³*National Research Centre "Kurchatov Institute", Moscow 123182, Russia*

We review studies of vortical motion and the resulting global polarization of Λ and $\bar{\Lambda}$ hyperons in heavy-ion collisions, in particular, within 3FD model. 3FD predictions for the global midrapidity polarization in the FAIR-NICA energy range are presented. The 3FD simulations indicate that energy dependence of the observed global polarization of hyperons in the midrapidity region is a consequence of the decrease of the vorticity in the central region with the collision energy rise because of pushing out the vorticity field into the fragmentation regions. At high collision energies this pushing-out results in a peculiar vortical structure consisting of two vortex rings: one ring in the target fragmentation region and another one in the projectile fragmentation region with matter rotation being opposite in these two rings.

PACS numbers: 25.75.-q, 25.75.Nq, 24.10.Nz

Keywords: relativistic heavy-ion collisions, hydrodynamics, vorticity

I. INTRODUCTION

Strongly interacting matter characterized by extremely high baryon and energy densities is created in heavy ion collisions at relativistic energies. This matter demonstrates strong collective behavior that is well described by relativistic hydrodynamics. The collective behavior is manifested in directed and elliptic flow [1, 2] that is comprehensively studied both experimentally and theoretically for a long time.

Non-central heavy-ion collisions at high energies are also characterized by a huge global angular momentum. This is illustrated in Fig. 1, where the total angular momentum (J_{total}) achieved in Au+Au collisions at impact parameter $b = 8$ fm is plotted as a function of the center-of-mass collision energy $\sqrt{s_{NN}}$. The calculations were performed within the model of the three-fluid dynamics (3FD) [3] with two versions of the equation of state (EoS) involving deconfinement transition [4], i.e. a first-order-phase-transition (1PT) EoS and a crossover EoS. As seen, J_{total} rapidly rises with the collision energy, exceeding the value of $10^5 \hbar$ at $\sqrt{s_{NN}} > 25$ GeV. It is independent of the used EoS. However, only a part of the total angular momentum is accumulated in the participant region, i.e. in the overlap region of the interacting nuclei, which is of prime interest for us. As seen from Fig. 1, 25–30% of the total angular momentum is deposited into the participant matter in the Au+Au collisions at $b = 8$ fm, which is also a huge amount. The participant angular momentum depends, though weakly, on the EoS because the overlap region of the interacting nuclei expands in the course of the collision, including more and more former spectators. The dynamics of this expansion depends on the EoS.

As the angular momentum is accumulated in the participant region, the motion of the matter becomes vor-

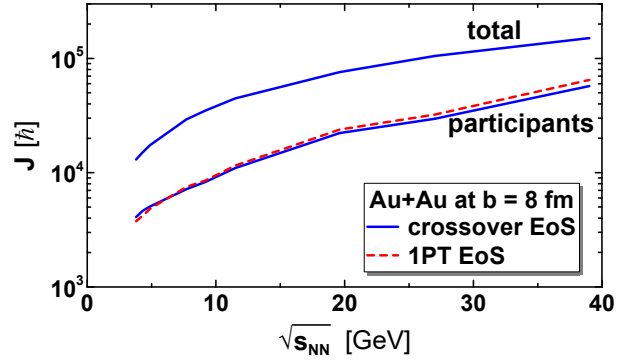


FIG. 1: The total angular momentum (conserved quantity) and the angular momentum accumulated in the participant region in semi-central ($b = 8$ fm) Au+Au collision as functions of $\sqrt{s_{NN}}$. Calculations are done within the 3FD model with the 1PT and crossover EoS's.

tical. In non-relativistic case it is characterized by the non-relativistic vorticity

$$\boldsymbol{\omega} = \frac{1}{2} \nabla \times \mathbf{v}, \quad (1)$$

where \mathbf{v} is a conventional collective 3-velocity of the matter. The relativistic generalization of this vorticity is

$$\omega_{\mu\nu} = \frac{1}{2} (\partial_\nu u_\mu - \partial_\mu u_\nu), \quad (2)$$

where u_μ is a collective local four-velocity of the matter.

The vortical motion significantly affects the evolution of the system. However, theoretical and experimental studies of the relevant effects began relatively recently. In particular, in Ref. [5] it was suggested that parton interaction in non-central heavy-ion collisions leads to a global quark polarization along the direction of the global angular momentum. This global polarization is essentially a local manifestation of the global angular momentum of the colliding system through spin-orbital coupling [6, 7].

*e-mail: yivanov@theor.jinr.ru

This phenomenon of the global polarization along the total angular momentum is closely related to the Barnett effect [8] (magnetization by rotation). The Barnett effect consists in transformation of a fraction of the orbital angular momentum associated with the body rotation into spin angular momenta of the atoms, which, on the average, are directed along the orbital angular momentum. Because of the proportionality between the spin and magnetic moment, this polarization results in a magnetization of the rotating body.

Measurement of the polarization of hadrons produced in heavy-ion collisions is not an easy task by itself. The most straightforward way to detect the global polarization in relativistic nuclear collisions is based on measuring polarization of Λ hyperons because they are so-called self-analyzing particles. The Λ hyperons decay weakly violating parity: $\Lambda \rightarrow p + \pi^-$ and $\bar{\Lambda} \rightarrow \bar{p} + \pi^+$. In the Λ rest frame the daughter proton is predominantly emitted along the Λ polarization (\mathbf{P}_Λ^*):

$$\frac{dN}{d\cos\theta^*} = \frac{1}{2}(1 + \alpha_\Lambda \mathbf{P}_\Lambda^* \cos\theta^*) \quad (3)$$

where $*$ means Λ 's rest frame, $\alpha_\Lambda = -\alpha_{\bar{\Lambda}} = 0.642$ is the Λ decay constant [9], and θ^* is the angle of the emitted proton. However, first measurements of the global polarization of Λ and $\bar{\Lambda}$ hyperons at $\sqrt{s_{NN}} = 62.4$ GeV and 200 GeV performed with the STAR detector at RHIC [10] showed result consistent with zero within the precision of the measurements. Later measurements by the STAR Collaboration gave nonzero values for the global polarization in the energy range $\sqrt{s_{NN}} = 7.7$ –200 GeV [11, 12], see Fig. 2. These results required more quantitative approaches to the calculation of the global polarization.

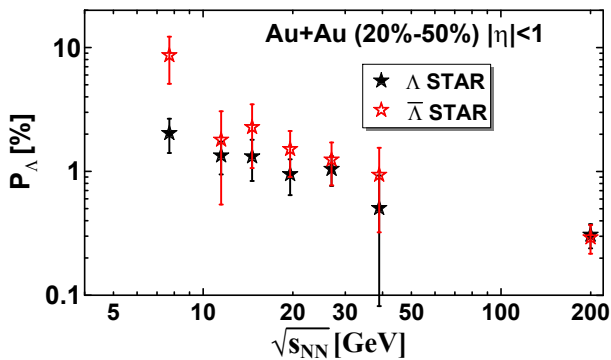


FIG. 2: Global polarization of Λ and $\bar{\Lambda}$ as a function of the collision energy $\sqrt{s_{NN}}$ for 20-50% centrality Au+Au collisions.

The most popular now thermodynamic approach to such calculations was proposed in Refs. [13, 14] and then further elaborated [15, 16]. More precisely, the derivation of Refs. [13, 14] was performed in terms of the hadronic degrees of freedom and for a (1/2)-spin particle. The thermodynamic approach does not require the precise form of the spin-orbital coupling. It requires only

the fact that such a coupling exists and its scale is the strong-interaction one. The latter is required for fast local equilibration of spin degrees of freedom similar to that for momentum degrees of freedom. Nevertheless, certain features of the spin-orbital coupling are silently assumed in the thermodynamic approach. In particular, this coupling is assumed to be the same for baryons and anti-baryons. Had it be a coupling because of induced magnetic field (like in the Barnett effect), polarizations of baryons and anti-baryons would be of opposite sign. All together, this makes possible a definite quantitative estimate of polarization through a suitable extension of the freeze-out formula.

The measured polarization is generally reproduced within the thermodynamics approach [14–16] implemented in hydrodynamic UrQMD+vHLLLE [17] and PICR [18] models, as well as kinetic AMPT [19–22] and PHSD [23] models. This reproduction indicates that our current understanding of the heavy-ion dynamics and, in particular, the vortical motion is compatible with observed polarization. However, a potential problem persists. The thermodynamic approach is unable to explain a big difference between polarization of Λ and $\bar{\Lambda}$ at 7.7 GeV. A possible source of this big difference could be magnetic field induced in the course of the collision because it results in opposite polarization of baryons and anti-baryons. This possibility was studied in Ref. [24]. It was found that there is no way to obtain the large splitting of the spin polarization between Λ and $\bar{\Lambda}$ at $\sqrt{s_{NN}} = 7.7$ GeV with partonic dynamics. It is not quite clear whether this contradiction between the predictions of the thermodynamics approach and the STAR data at energy of 7.7 GeV really takes place because of large error bars of the measured $\bar{\Lambda}$ polarization. More accurate measurements are needed to clarify this problem.

However, there are approaches which naturally explain this difference. One of them is that directly based on the axial vortical effect [25–27]. The axial vortical effect is associated with axial-vector current induced by vorticity. This current implies that the right (left)-handed fermions move parallel (opposite) to the direction of vorticity. As the momentum of a right (left)-handed massless fermion is parallel (opposite) to its spin, all spins become parallel to the direction of vorticity, i.e. aligned. Application of this approach with parameters deduced from the quark-gluon string transport model [28] well reproduces both the $\bar{\Lambda}$ and Λ polarizations and splitting between them. Another recently suggested approach [29] based on a Walecka-like model can also explain the difference in the $\bar{\Lambda}$ - Λ polarizations. However, ability of this Walecka-like approach to describe absolute values of these polarizations still remains to be seen.

The problem of relation between the vorticity and spin-polarization tensor in relativistic systems is far from being completely solved. The thermodynamic derivation the spin polarization in Refs. [13–15] is not completely consistent. The author themselves call it an educated ansatz [30]. A critical review of this issue is presented in

Ref. [31].

In the present paper we review studies of vortical motion and the resulting global polarization of Λ and $\bar{\Lambda}$ hyperons in Au+Au collisions performed within the 3FD model [32–34]. The 3FD model describes of the major part of bulk observables: the baryon stopping [35, 36], yields of different hadrons, their rapidity and transverse momentum distributions [37, 38], and also the elliptic [39] and directed [40] flow. It also reproduces [41] recent STAR data on bulk observables [42]. We also address the question why the observed global polarization of hyperons in the midrapidity region, i.e. at pseudorapidity $|\eta| < 1$ (see Fig. 2), drops with the collision energy rise while the angular momentum accumulated in the system substantially increases (see Fig. 1) at the same time?

II. VORTICITY IN THE 3FD MODEL

The 3FD model takes into account a finite stopping power resulting in counterstreaming of leading baryon-rich matter at early stage of nuclear collisions [3]. This nonequilibrium stage is modeled by means of two counterstreaming baryon-rich fluids initially associated with constituent nucleons of the projectile (p) and target (t) nuclei. Later on these fluids may consist of any type of hadrons and/or partons (quarks and gluons), rather than only nucleons. Newly produced particles, dominantly populating the midrapidity region, are associated with a fireball (f) fluid. These fluids are governed by conventional hydrodynamic equations coupled by friction terms in the right-hand sides of the Euler equations. The friction results in energy–momentum loss of the baryon-rich fluids. A part of this loss is transformed into thermal excitation of these fluids, while another part leads to formation of the fireball fluid. Thus, the 3FD approximation is a minimal way to implement the early-stage nonequilibrium of the produced strongly-interacting matter at high collision energies.

Three different equations of state (EoS's) were used in simulations of Refs. [35–41]: a purely hadronic EoS [43] and two versions of the EoS with the deconfinement transition [4], i.e. a first-order phase transition and a crossover one. In the present review only the first-order-phase-transition (1PT) and crossover EoS's are discussed as the most relevant to various observables.

A so-called thermal vorticity is defined as

$$\varpi_{\mu\nu} = \frac{1}{2}(\partial_\nu \hat{\beta}_\mu - \partial_\mu \hat{\beta}_\nu), \quad (4)$$

where $\hat{\beta}_\mu = \hbar\beta_\mu$, $\beta_\mu = u_\nu/T$, u_μ is collective local four-velocity of the matter, and T is local temperature. In the thermodynamical approach [14–16] in the leading order in the thermal vorticity it is directly related to the mean spin vector of spin 1/2 particles with four-momentum p , produced around point x on freeze-out hypersurface

$$S^\mu(x, p) = \frac{1}{8m}[1 - n_F(x, p)] p_\sigma \epsilon^{\mu\nu\rho\sigma} \varpi_{\rho\nu}(x) \quad (5)$$

where $n_F(x, p)$ is the Fermi-Dirac distribution function and m is mass of the considered particle. To calculate the relativistic mean spin vector of a given particle species with given momentum, the above expression should be integrated over the freeze-out hypersurface. Therefore, we proceed to discussion in terms of the thermal vorticity.

Unlike the conventional hydrodynamics, the system is characterized by three hydrodynamical velocities, u_a^μ ($a = p, t$ and f), in the 3FD model. The counterstreaming of the p and t fluids takes place only at the initial stage of the nuclear collision that lasts from ~ 5 fm/c at $\sqrt{s_{NN}} = 5$ GeV [32] to ~ 1 fm/c at collision energy of 39 GeV [44]. At later stages the baryon-rich (p and t) fluids have already either partially passed through each other or partially stopped and unified in the central region. Therefore, after the initial thermalization stage the system is characterized by two hydrodynamical velocities, u_B^μ and u_f^μ , and two temperatures, T_B and T_f , corresponding to the unified baryon-rich (B) and fireball (f) fluids.

As a result the system is characterized by two sets of the vorticity related to these baryon-rich and baryon-free fluids, $\varpi_{\mu\nu}^B$ and $\varpi_{\mu\nu}^f$, respectively. In order to define a single quantity responsible for the particle polarization we make sum of these vorticities with the weights of their energy densities

$$\tilde{\varpi}_{\mu\nu}(\mathbf{x}, t) = \frac{\varpi_{\mu\nu}^B(\mathbf{x}, t)\varepsilon_B(\mathbf{x}, t) + \varpi_{\mu\nu}^f(\mathbf{x}, t)\varepsilon_f(\mathbf{x}, t)}{\varepsilon(\mathbf{x}, t)} \quad (6)$$

where ε_B and ε_f are the proper (i.e. in the local rest frame) energy densities of the baryon-rich and baryon-free fluids, respectively, and ε is proper energy density of all three fluids in their combined local rest frame. In view of almost perfect unification of the baryon-rich fluids and small local baryon-fireball relative velocities [44] at the later stages of the collision, a very good approximation for ε is just

$$\varepsilon \simeq \varepsilon_B + \varepsilon_f. \quad (7)$$

The proper-energy-density weighted vorticity allows us to suppress contributions of regions of low-density matter. It is appropriate because production of (anti)hyperons under consideration dominantly takes place in highly excited regions of the system.

In Fig. 3, the proper-energy-density weighted thermal zx vorticity of the baryon-rich subsystem in the reaction plane (xz) is presented at various time instants in semi-central ($b = 6$ fm) Au+Au collisions at $\sqrt{s_{NN}} = 7.7$ GeV. As seen, the thermal vorticity primarily starts at the border between the participant and spectator matter. Later on it partially spreads to the participant and spectator bulk though remain concentrated near the border. In the conventional hydrodynamics this extension into the bulk of the system is an effect of the shear viscosity. In the 3FD dynamics it is driven by the 3FD dissipation which imitates the effect of the shear viscosity [45]. The spread into the bulk, i.e. into the midrapidity region,

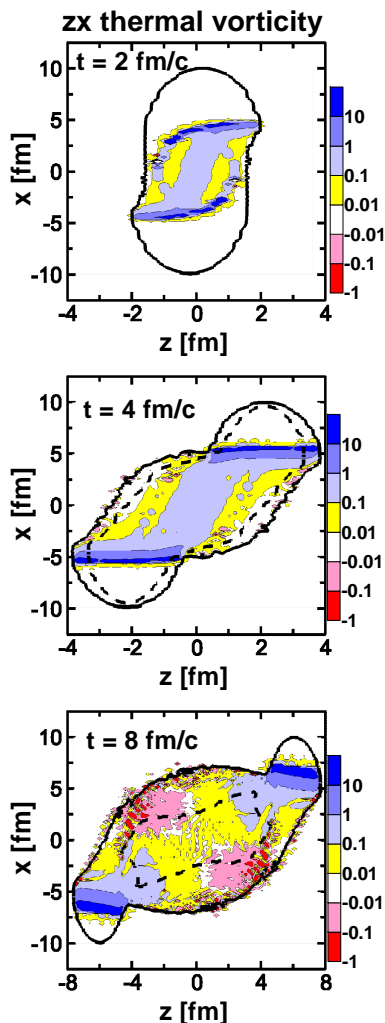


FIG. 3: The proper-energy-density weighted thermal zx vorticity of the baryon-rich subsystem, in the reaction plane at various time instants in the semi-central ($b = 6$ fm) Au+Au collision at $\sqrt{s_{NN}} = 7.7$ GeV. Calculations are done with the crossover EoS. z axis is the beam direction. Note different scale along the z axis at different time instants. The outer bold solid contour displays the border of the baryon-rich matter. Inside this contour $n_B/n_0 > 0.1$. The inner bold dashed contour indicates the freeze-out border. Inside this contour the matter still hydrodynamically evolves, while outside – it is frozen out. At $t = 2$ and 4 fm/c there is no frozen-out matter.

is stronger at lower collision energies [32] because of the higher effective shear viscosity than that at higher energies [45]. This explains the drop of the vorticity value and consequently the observed hyperon polarization at the midrapidity with the collision energy rise.

At later times the maximum values in the vortical fields get more and more shifted to the fragmentation regions because of the 1D expansion of the system. At the same time, the vorticity in the participant bulk gradually dissolves. It is peculiarly that four strong oppositely directed vortices are formed at the periphery of the frag-

mentation regions, see Fig. 3. The vortex at the border with the spectator matter is an order of magnitude stronger than its counterpart. This is the structure as it is seen in the reaction plane.

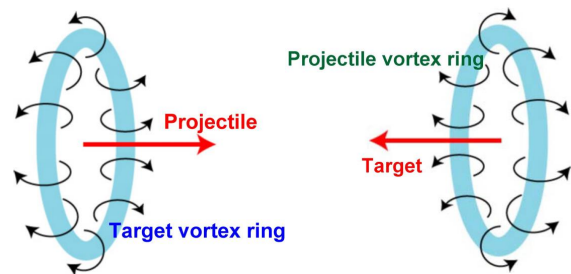


FIG. 4: Schematic picture of the vortex rings in the fragmentation regions. Curled arrows indicate direction of the circulation of the target matter.

In fact, in three dimensions these are two vortex rings: one in the target fragmentation region and another in the projectile one. The matter rotation is opposite in these two rings. They are formed because the matter in the vicinity of the beam axis (z) is stronger decelerated because of thicker matter in the center than that at the periphery. Indeed, these rings are formed at the transverse periphery of the stopped matter in the central region, see the central bumps in n_B and ε at $t = 1$ fm/c in Fig. 3. Thus, the peripheral matter acquires a rotational motion. A schematic picture of these vortex rings in the fragmentation regions is presented in Fig. 4.

A similar effect was noticed in the analysis of the vorticity field [46, 47] at lower NICA energies. The authors of Refs. [46, 47] called this specific toroidal structure as a femto-vortex sheet. This femto-vortex sheet is not a ring because the vorticity disappears in the xy plane, i.e. in the plane orthogonal to the reaction xz plane. At higher collision energies this femto-vortex sheet splits into two real rings.

These rings are also formed in central collisions, as seen from Fig. 5. As seen, the vortex rings are formed already at $t = 1$ fm/c. In fact, the schematic picture of the completely symmetric vortex ring, see Fig. 4, corresponds to the exactly central collision at $b = 0$.

Figure 5 presents the time evolution of the proper-energy-density weighted thermal zx vorticity in the reaction plain ($x\eta_s$) of central Au+Au collision at $\sqrt{s_{NN}} = 39$ GeV, where

$$\eta_s = \frac{1}{2} \ln \left(\frac{t+z}{t-z} \right) \quad (8)$$

is the longitudinal space-time rapidity and z is the coordinate along the beam direction. The advantage of this longitudinal space-time rapidity is that it zooms Lorentz-contracted regions.

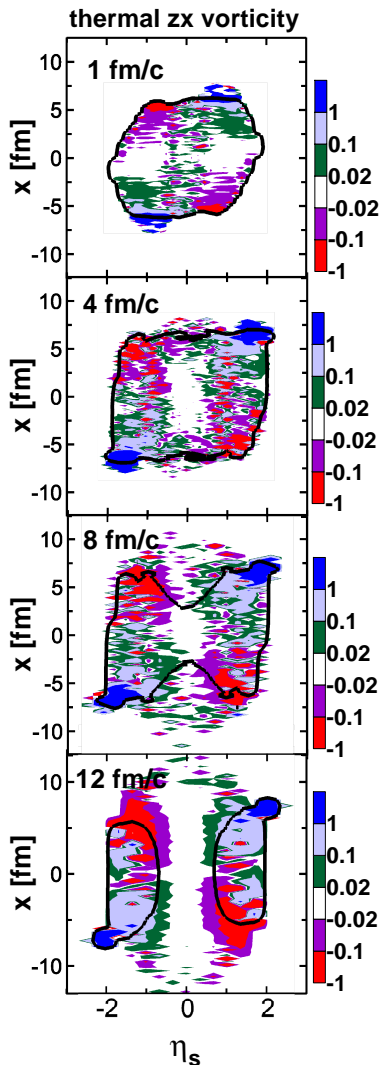


FIG. 5: The proper-energy-density weighted thermal zx vorticity in the central ($b = 2$ fm) Au+Au collision at $\sqrt{s_{NN}} = 39$ GeV. η_s is the space-time rapidity along the beam direction, see Eq. (8). Calculations are done with the 1PT EoS. The bold solid contour displays the border of the frozen out matter. Inside this contour the matter still hydrodynamically evolves, while outside – it is frozen out.

III. POLARIZATION

The above observation of pushing out the vortical field to the fragmentation regions has consequence for the polarization of produced particles. The polarized particles dominantly originate from peripheral regions with high vorticity, see right panel in Fig. 3 and Fig. 5. Therefore, the relative polarization of Λ hyperons should be higher in the fragmentation regions, i.e. the kinematical region of the participant-spectator border, than that in the midrapidity region.

In terms of the mean spin vector (5), the polarization

vector of S -spin particle is defined as

$$P_S^\mu = S^\mu / S. \quad (9)$$

In the experiment, the polarization of the Λ hyperon is measured in its rest frame, therefore the Λ polarization is

$$P_\Lambda^\mu = 2S_\Lambda^{*\mu} \quad (10)$$

where $S_\Lambda^{*\mu}$ is mean spin vector of the Λ hyperon in its rest frame. Substituting expression for \mathbf{S} from Eq. (5) and averaging it over the \mathbf{p}_Λ direction (i.e. over \mathbf{n}_p) we arrive at the following polarization along the y axis [23] (see also [14–16])

$$\langle P_\Lambda \rangle_{\mathbf{n}_p} = \frac{1}{2m_\Lambda} \left(E_\Lambda - \frac{1}{3} \frac{\mathbf{p}_\Lambda^2}{E_\Lambda + m_\Lambda} \right) \varpi_{zx}, \quad (11)$$

where m_Λ is the Λ mass, E_Λ and \mathbf{p}_Λ are the energy and momentum of the emitted Λ hyperon, respectively. Here we put $(1 - n_\Lambda) \simeq 1$ because the Λ production takes place only in high-temperature regions, where Boltzmann statistics dominates.

We apply further approximations after which the present evaluation of the global polarization becomes more an estimation rather than a calculation. We associate the global midrapidity polarization with the polarization of Λ hyperons emitted from the central region (i.e. central slab) of colliding system, see details in Ref. [34]. We decouple averaging of ϖ_{zx} and the term in parentheses in Eq. (11). Neglecting the longitudinal motion of the Λ hyperon in the central slab, we approximate the average Λ energy by the mean midrapidity transverse mass: $\langle E_\Lambda \rangle = \langle m_T^\Lambda \rangle_{\text{midrap.}}$, which was calculated earlier in Ref. [38]. Thus we arrive at the estimate of the global midrapidity Λ -polarization in the y direction

$$\langle P_\Lambda \rangle_{\text{midrap.}} \simeq \frac{\langle \varpi_{zx} \rangle_{\text{cent. slab}}}{2} \left(1 + \frac{2}{3} \frac{\langle m_T^\Lambda \rangle_{\text{midrap.}} - m_\Lambda}{m_\Lambda} \right) \quad (12)$$

Results of this estimate are presented in panel (a) of Fig. 6. The corresponding 3FD simulations of Au+Au collisions were performed at fixed impact parameters $b = 8$ fm. This value of b was chosen in order to roughly comply with the centrality selection 20-50% in the STAR experiment [11]. The correspondence between experimental centrality and the mean impact parameter was taken from Glauber simulations of Ref. [48].

As seen from Fig. 6, such a rough estimate of the global midrapidity polarization quite satisfactorily reproduces the experimental data, especially the collision-energy dependence of the polarization. This energy dependence is related to the above discussed decrease of the thermal vorticity in the central region with the collision energy rise. The performed estimate predicts that the global midrapidity polarization further increases at NICA/FAIR energies, reaching values of 5% at $\sqrt{s_{NN}} =$

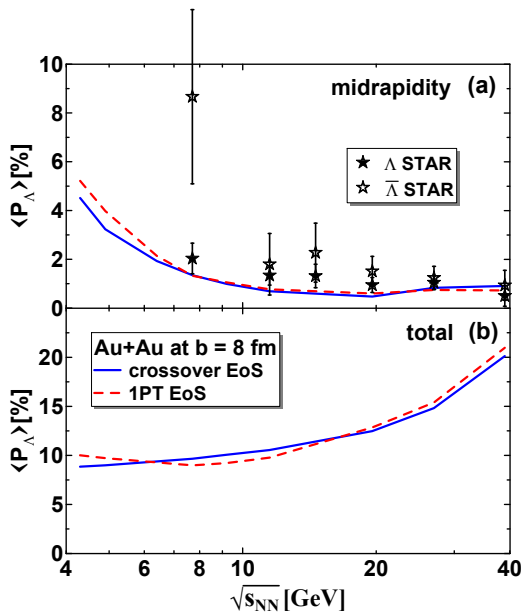


FIG. 6: Global (a), i.e. in the central region, and total (b), i.e. averaged over the whole participant region, polarization of Λ hyperons in Au+Au collisions at $b = 8$ fm as a function of collision energy $\sqrt{s_{NN}}$. STAR data on global Λ and also $\bar{\Lambda}$ polarization in the midrapidity region (pseudorapidity cut $|\eta| < 1$) [11] are also displayed.

3.8 GeV. This prediction approximately agrees with that made in Ref. [28] based on the axial vortical effect [25–27].

The global midrapidity polarization of $\bar{\Lambda}$ hyperons differs only by replacement of $\langle m_T^\Lambda \rangle_{\text{midrap.}}$ by $\langle m_T^{\bar{\Lambda}} \rangle_{\text{midrap.}}$ in Eq. (12) from that for Λ 's and quantitatively does not exceed 5% of that for Λ hyperons. Therefore, we do not display it in Fig. 6. Uncertainties of this estimate were discussed in Ref. [34]. These were found to be of the order of 20%, of course excluding the main uncertainty associated with decoupling of averaging of ϖ_{zx} and the term in parentheses in Eq. (11).

In the case of total Λ polarization, the averaging runs over the whole participant region. In such averaging the above applied decoupling of averaging of ϖ_{zx} and the term in parentheses in Eq. (11) is even less justified than in the central region. Therefore, we do even more rough estimate of the mean total polarization of emitted Λ hyperons

$$\langle P_\Lambda \rangle_{\text{total}} \approx \frac{\langle \varpi_{zx} \rangle}{2} \quad (13)$$

by neglecting the term in parentheses in Eq. (11). Note that this term is a correction, though not a negligible one. Sometimes it results in 30% correction for the central-slab polarization.

Results of this estimate of the total Λ polarization are presented in panel (b) of Fig. 6. The total Λ polarization increases with collision energy rise. This is in contrast to

the energy dependence of the midrapidity polarization. This increase is quite moderate as compared with the rapid rise of the angular momentum accumulated in the participant region, see Fig. 1. The increase of the total polarization with simultaneous decrease of the midrapidity one suggests that the Λ polarization in the fragmentation regions reaches high values at high collision energies. At lower collision energies values of the total and midrapidity polarization are close to each other, which reflects a more homogeneous distribution of the vortical field over the bulk of the produced matter.

IV. SUMMARY

We reviewed studies of the vortical motion and the resulting global polarization of Λ and $\bar{\Lambda}$ hyperons in heavy-ion collisions, in particular, within the 3FD model [32–34]. The measurement of the polarization give us possibility to deduce information on the vortical motion of the matter produced in heavy-ion collisions. The interrelation between the vortical motion and the polarization is not quite clear at present. Calculations of the global polarization of Λ and $\bar{\Lambda}$ hyperons based on the thermodynamics approach [14–16] implemented within various models [17–23, 34], including the 3FD one, are consistent with data by the STAR Collaboration in the energy range $\sqrt{s_{NN}} = 7.7$ –200 GeV [11, 12]. However, the thermodynamic approach is unable to explain a big difference between polarization of Λ and $\bar{\Lambda}$ at 7.7 GeV. It should be mentioned that there are alternative approaches [25–29], which naturally explain this difference. In view of large error bars of the measured $\bar{\Lambda}$ polarization at this energy, more accurate measurements are needed to clarify this problem.

Based on the analysis within the 3FD model [34] predictions are made for the global midrapidity polarization in the FAIR-NICA [49, 50] energy range. The performed estimate predicts that the global midrapidity polarization further increases at NICA/FAIR energies, reaching values of 5% at $\sqrt{s_{NN}} = 3.8$ GeV. This prediction approximately agrees with that made in Ref. [28] based on the axial vortical effect [25–27].

It is found that the energy dependence the observed global polarization of hyperons in the midrapidity region is a consequence of the decrease of the thermal vorticity in the central region with the collision energy rise, which in its turn results from pushing out the vorticity field into the fragmentation regions [33, 51].

At high collision energies $\sqrt{s_{NN}} \gtrsim 8$ GeV, this pushing-out results in a peculiar vortical structure consisting of two vortex rings: one ring in the target fragmentation region and another one in the projectile fragmentation region with the matter rotation being opposite in these two rings [33], see Fig. 4. These vortex rings produce very strong Λ polarization in the fragmentation

regions at noncentral collisions.

Acknowledgments

The problems considered in this contribution have been repeatedly discussed with E. E. Saperstein. We are very grateful to him for these discussions. Fruitful discussions with E. E. Kolomeitsev and O. V. Teryaev are gratefully acknowledged. This work was carried out using computing resources of the federal collective usage center “Complex for simulation and data process-

ing for mega-science facilities” at NRC “Kurchatov Institute”, <http://ckp.nrcki.ru/>. Y.B.I. was supported by the Russian Science Foundation, Grant No. 17-12-01427, and the Russian Foundation for Basic Research, Grants No. 18-02-40084 and No. 18-02-40085. A.A.S. was partially supported by the Ministry of Education and Science of the Russian Federation within the Academic Excellence Project of the NRNU MEPhI under contract No. 02.A03.21.0005.

-
- [1] S. Voloshin and Y. Zhang, *Z. Phys. C* **70**, 665 (1996).
- [2] S. A. Voloshin, A. M. Poskanzer and R. Snellings, in *Landolt-Boernstein New Series, I/23*, p. 5-54, edited by R. Stock (Springer-Verlag, 2010).
- [3] Yu. B. Ivanov, V. N. Russkikh, and V.D. Toneev, *Phys. Rev. C* **73**, 044904 (2006) [nucl-th/0503088].
- [4] A. S. Khvorostukhin, V. V. Skokov, K. Redlich, and V. D. Toneev, *Eur. Phys. J. C* **48**, 531 (2006) [nucl-th/0605069].
- [5] Z. T. Liang and X. N. Wang, *Phys. Rev. Lett.* **94**, 102301 (2005) Erratum: [*Phys. Rev. Lett.* **96**, 039901 (2006)] [nucl-th/0410079].
- [6] B. Betz, M. Gyulassy and G. Torrieri, *Phys. Rev. C* **76**, 044901 (2007) [arXiv:0708.0035 [nucl-th]].
- [7] J. H. Gao, S. W. Chen, W. t. Deng, Z. T. Liang, Q. Wang and X. N. Wang, *Phys. Rev. C* **77**, 044902 (2008) [arXiv:0710.2943 [nucl-th]].
- [8] S. J. Barnett, *Phys. Rev.* **6**, 239 (1915).
- [9] M. Tanabashi *et al.* [Particle Data Group], *Phys. Rev. D* **98**, no. 3, 030001 (2018).
- [10] B. I. Abelev *et al.* [STAR Collaboration], *Phys. Rev. C* **76**, 024915 (2007) Erratum: [*Phys. Rev. C* **95**, no. 3, 039906 (2017)] [arXiv:0705.1691 [nucl-ex]].
- [11] L. Adamczyk *et al.* [STAR Collaboration], *Nature* **548**, 62 (2017) [arXiv:1701.06657 [nucl-ex]].
- [12] J. Adam *et al.* [STAR Collaboration], *Phys. Rev. C* **98**, 014910 (2018) [arXiv:1805.04400 [nucl-ex]].
- [13] F. Becattini and F. Piccinini, *Annals Phys.* **323**, 2452 (2008) [arXiv:0710.5694 [nucl-th]].
- [14] F. Becattini, V. Chandra, L. Del Zanna and E. Grossi, *Annals Phys.* **338**, 32 (2013) [arXiv:1303.3431 [nucl-th]].
- [15] F. Becattini, I. Karpenko, M. Lisa, I. Uppsala and S. Voloshin, *Phys. Rev. C* **95**, no. 5, 054902 (2017) [arXiv:1610.02506 [nucl-th]].
- [16] R. h. Fang, L. g. Pang, Q. Wang and X. n. Wang, *Phys. Rev. C* **94**, no. 2, 024904 (2016) [arXiv:1604.04036 [nucl-th]].
- [17] I. Karpenko and F. Becattini, *Eur. Phys. J. C* **77**, no. 4, 213 (2017) [arXiv:1610.04717 [nucl-th]].
- [18] Y. Xie, D. Wang and L. P. Csernai, *Phys. Rev. C* **95**, no. 3, 031901 (2017) [arXiv:1703.03770 [nucl-th]].
- [19] H. Li, L. G. Pang, Q. Wang and X. L. Xia, *Phys. Rev. C* **96**, no. 5, 054908 (2017) [arXiv:1704.01507 [nucl-th]].
- [20] Y. Sun and C. M. Ko, *Phys. Rev. C* **96**, no. 2, 024906 (2017) [arXiv:1706.09467 [nucl-th]].
- [21] D. X. Wei, W. T. Deng and X. G. Huang, *Phys. Rev. C* **99**, no. 1, 014905 (2019) [arXiv:1810.00151 [nucl-th]].
- [22] S. Shi, K. Li and J. Liao, *Phys. Lett. B* **788**, 409 (2019) [arXiv:1712.00878 [nucl-th]].
- [23] E. E. Kolomeitsev, V. D. Toneev and V. Voronyuk, *Phys. Rev. C* **97**, no. 6, 064902 (2018) [arXiv:1801.07610 [nucl-th]].
- [24] Z. Z. Han and J. Xu, *Phys. Lett. B* **786**, 255 (2018) [arXiv:1707.07262 [nucl-th]].
- [25] O. Rogachevsky, A. Sorin and O. Teryaev, *Phys. Rev. C* **82**, 054910 (2010) [arXiv:1006.1331 [hep-ph]].
- [26] J. H. Gao, Z. T. Liang, S. Pu, Q. Wang and X. N. Wang, *Phys. Rev. Lett.* **109**, 232301 (2012) [arXiv:1203.0725 [hep-ph]].
- [27] A. Sorin and O. Teryaev, *Phys. Rev. C* **95**, no. 1, 011902 (2017) [arXiv:1606.08398 [nucl-th]].
- [28] M. Baznat, K. Gudima, A. Sorin and O. Teryaev, *Phys. Rev. C* **97**, no. 4, 041902 (2018) [arXiv:1701.00923 [nucl-th]].
- [29] L. P. Csernai, J. I. Kapusta and T. Welle, *Phys. Rev. C* **99**, no. 2, 021901 (2019) [arXiv:1807.11521 [nucl-th]].
- [30] F. Becattini, *Nucl. Phys. A* **982**, 57 (2019) [arXiv:1810.02706 [nucl-th]].
- [31] W. Florkowski, A. Kumar and R. Ryblewski, *Phys. Rev. C* **98**, no. 4, 044906 (2018) [arXiv:1806.02616 [hep-ph]].
- [32] Y. B. Ivanov and A. A. Soldatov, *Phys. Rev. C* **95**, no. 5, 054915 (2017) [arXiv:1701.01319 [nucl-th]].
- [33] Y. B. Ivanov and A. A. Soldatov, *Phys. Rev. C* **97**, no. 4, 044915 (2018) [arXiv:1803.01525 [nucl-th]].
- [34] Y. B. Ivanov, V. D. Toneev and A. A. Soldatov, *arXiv:1903.05455 [nucl-th]*.
- [35] Yu. B. Ivanov, *Phys. Rev. C* **87**, 064904 (2013) [arXiv:1302.5766 [nucl-th]].
- [36] Y. B. Ivanov, *Phys. Lett. B* **721**, 123 (2013) [arXiv:1211.2579 [hep-ph]]; Y. B. Ivanov and D. Blaschke, *Phys. Rev. C* **92**, no. 2, 024916 (2015) [arXiv:1504.03992 [nucl-th]].
- [37] Y. B. Ivanov, *Phys. Rev. C* **87**, no. 6, 064905 (2013) [arXiv:1304.1638 [nucl-th]].
- [38] Y. B. Ivanov, *Phys. Rev. C* **89**, no. 2, 024903 (2014) [arXiv:1311.0109 [nucl-th]].
- [39] Y. B. Ivanov and A. A. Soldatov, *Phys. Rev. C* **91**, no. 2, 024914 (2015) [arXiv:1401.2265 [nucl-th]]; Y. B. Ivanov, *Phys. Lett. B* **723**, 475 (2013) [arXiv:1304.2307 [nucl-th]].
- [40] V. P. Konchakovski, W. Cassing, Y. B. Ivanov and V. D. Toneev, *Phys. Rev. C* **90**, no. 1, 014903 (2014) [arXiv:1404.2765 [nucl-th]]; Y. B. Ivanov and A. A. Soldatov, *Phys. Rev. C* **91**, no. 2, 024915 (2015) [arXiv:1412.1669 [nucl-th]]; *Eur. Phys. J. A* **52**, no. 1, 10 (2016) [arXiv:1601.03902 [nucl-th]].
- [41] Y. B. Ivanov and A. A. Soldatov, *Phys. Rev. C* **97**, no. 2, 024908 (2018) [arXiv:1801.01764 [nucl-th]].

- [42] L. Adamczyk *et al.* [STAR Collaboration], Phys. Rev. C **96**, no. 4, 044904 (2017) [arXiv:1701.07065 [nucl-ex]].
- [43] V. M. Galitsky and I. N. Mishustin, Sov. J. Nucl. Phys. **29**, 181 (1979).
- [44] Y. B. Ivanov and A. A. Soldatov, Phys. Rev. C **97**, no. 2, 021901 (2018) [arXiv:1711.03069 [nucl-th]]; Phys. Rev. C **98**, no. 1, 014906 (2018) [arXiv:1803.11474 [nucl-th]].
- [45] Y. B. Ivanov and A. A. Soldatov, Eur. Phys. J. A **52**, no. 5, 117 (2016) [arXiv:1604.03261 [nucl-th]]; Eur. Phys. J. A **52**, no. 12, 367 (2016) [arXiv:1605.02476 [nucl-th]].
- [46] M. I. Baznat, K. K. Gudima, A. S. Sorin and O. V. Teryaev, Phys. Rev. C **93**, no. 3, 031902 (2016) [arXiv:1507.04652 [nucl-th]].
- [47] M. Baznat, K. Gudima, A. Sorin and O. Teryaev, Phys. Rev. C **88**, no. 6, 061901 (2013) [arXiv:1301.7003 [nucl-th]].
- [48] B. I. Abelev *et al.* [STAR Collaboration], Phys. Rev. C **79**, 034909 (2009) [arXiv:0808.2041 [nucl-ex]].
- [49] B. Friman, C. Hohne, J. Knoll, S. Leupold, J. Randrup, R. Rapp and P. Senger, Lect. Notes Phys. **814**, pp.1 (2011).
- [50] V. D. Kekelidze, V. A. Matveev, I. N. Meshkov, A. S. Sorin and G. V. Trubnikov, Phys. Part. Nucl. **48**, no. 5, 727 (2017). V. D. Kekelidze, R. Lednicky, V. A. Matveev, I. N. Meshkov, A. S. Sorin and G. V. Trubnikov, Eur. Phys. J. A **52**, no. 8, 211 (2016).
- [51] Y. Jiang, Z. W. Lin and J. Liao, Phys. Rev. C **94**, no. 4, 044910 (2016) Erratum: [Phys. Rev. C **95**, no. 4, 049904 (2017)] [arXiv:1602.06580 [hep-ph]].